Journal of Applied Polymer Science

Double-Hydrophilic Polyether Antiscalant Used as a Crystal Growth Modifier of Calcium Scales in Cooling-Water Systems

Yahui Liu,[1] Yuming Zhou,[1] Qingzhao Yao,[1] Jingyi Huang,[1] Guangqing Liu,[1,2] Huchuan Wang,[1] Ke Cao,[1] Yiyi Chen,[1] Yunyun Bu,[1] Wendao Wu,[3] Wei Sun[3]

[1]School of Chemistry and Chemical Engineering, Southeast University, Nanjing 211189, People's Republic of China

[2]School of Biochemical and Environmental Engineering, Nanjing Xiaozhuang University, Nanjing 211171, People's Republic of China

[3]Jianghai Environmental Protection Company, Limited, Changzhou 213116, People's Republic of China

Correspondence to: Y. Zhou (E-mail: ymzhou@seu.edu.cn) or Q. Yao (E-mail: 101006377@seu.edu.cn)

ABSTRACT: In this study, we synthesized a novel double-hydrophilic poly(ethylene glycol) (PEG)-based crystal growth modifier polyethylene glycol double-ester of maleic anhydride/acrylic acid named PEGDMA/AA, whose structure was still linear but also had some differences from a traditional chelating linear polymer, in which the PEG segment was incorporated. The scale inhibition behavior of PEGDMA/AA was evaluated by means of a static scale inhibition method. As the polymerization degree of PEG_nDMA was 8 ($n = 8$), the maximum inhibitory toward calcium carbonate ($CaCO_3$) and calcium sulfate ($CaSO_4$) were 89.0 and 98.8% at dosage levels of 12 and 3 mg/L, respectively. Comparisons with other inhibitors were also carried out. Characterization of the $CaCO_3$ and $CaSO_4$ scales with scanning electron microscopy and transmission electron microscopy proved that great changes in the size and morphology of the calcium scales took place under the influence of PEG_8DMA/AA. X-ray diffraction and diffraction patterns further confirmed the impact of PEG_8DMA/AA as a crystal growth modifier. The three supposed mechanisms, (1) chelating solubilization, (2) multilayer type of adsorption, and (3) electrostatic repulsion function, are also described in detail. © 2013 Wiley Periodicals, Inc. J. Appl. Polym. Sci. **2014**, *131*, 39792.

KEYWORDS: applications; crystallization; hydrophilic polymers; recycling; self-assembly

Received 30 May 2013; accepted 23 July 2013

DOI: 10.1002/app.39792

INTRODUCTION

In recent years, the rapid development of modern industry has brought about great problems and concerns, such as the increasing consumption and pollution of water resources, which aggravate the shortage of fresh water. Limited by the shortage of water resources and to cut down its depletion, a recycling circulate water system has replaced the once-through cooling-water system.[1,2] In the long-cycle operation, severe phenomena of scale deposition, metal pipeline corrosion, microbial propagation occurred spontaneously; this caused security issues and technical and economic problems such as decreased system heat-transfer efficiency, increased cleaning frequency, and even unexpected system shutdowns.[3,4] To alleviate and prevent the aforementioned phenomena from occurring, the most common and effective control method is to apply water-treatment agents, which consist of strong chelating functional groups and pose superior affinity and dispersion power toward Ca^{2+}, Fe^{3+}, Mg^{2+}, Ba^{2+}, and the like in industrial water systems.[5] Polycarboxylate and polyphosphonate antiscalants are the most commonly used inhibitors for retarding the growth of calcium salts, such as poly(acrylic acid) (PAA), hydrolytic poly(maleic anhydride) (HPMA), 2-phosphonobutane 1,2,4-tricarboxylic acid (PBTC), 1-hydroxyethylidine 1,1-diphosphonic acid (HEDP), and poly(hydric alcohol phosphate ester), together with the nonphosphorus environmentally friendly inhibitor poly(epoxysuccinic acid) (PESA).[6–10] However, the currently used water treatments are endowed with unsatisfactory overall performances. Polycarboxylate inhibitors have a low calcium tolerance to form insoluble calcium–polymer salts, and their bad degradability results in a long period of existence after discharge, whereas the polyphosphate itself can hydrolyze into orthophosphate readily and form insoluble calcium phosphate and ferric phosphate scales with Ca^{2+} and Fe^{2+}/Fe^{3+} ions.[11] In addition to these disadvantages, inhibitors consisting of phosphorous are potential nutrients for algae and can lead to the water eutrophication after emission; this causes secondary pollution, which is also a great concern and challenge for environmental protection.[12] High levels of phosphonates are becoming increasingly restricted in terms of release into the environment. Therefore, the search for antiscalants posing not only wonderful scale inhibition qualities but also being

environment accepted is attracting the interest of scientific experts and technology workers.[13]

Corresponding to the environment guidelines and the criteria of green chemistry, calcium phosphate scales will be not the major deposition in industrial circulating-water systems. Alkaline scales calcium carbonate ($CaCO_3$) precipitate onto the internal walls of metal pipelines to form an insulated mineral layer; this depends on the saturation index of the water conditions, which is the predominantly generated scale. Factors such as temperature, CO_2, pH, evaporation of the solution, dissolved gases, microorganisms, fluid flow rate, and algae can all influence the formation of supersaturation degree and thus accelerate or retard the agglomeration of scales.[14] There are three crystal forms of $CaCO_3$: calcite, with a cubic shape or entangled rhombohedral shape; aragonite; and vaterite, with needle and flower-like structures.[14–16] Of the three crystal forms, calcite is the most thermodynamically stable under ambient conditions, but the less stable aragonite and/or vaterite phase can also be observed in the presence of inhibitors.[17] Conventionally, minerals can be gotten rid of by acid picking with sulfuric acid with the solution pH value maintained below 7.5. However, such methods increase the potential crystal growth of calcium sulfate ($CaSO_4$), which is not desired, because once deposited, $CaSO_4$ is hard to remove.[18,19] Meanwhile, acid can result in the corrosion of metal tubes and the deterioration of heat exchangers, which turn into an additional source of fouling.[20] $CaSO_4$ crystallizes out of water in three forms: dihydrate ($CaSO_4{\cdot}2H_2O$, gypsum), hemihydrate ($CaSO_4{\cdot}0.5H_2O$, Plaster of Paris), and anhydrite ($CaSO_4$), among which the former type is widely occurring on the heat-transfer surface. The relation between the solubility of $CaCO_3$, $CaSO_4$, and temperature is inverse; that is, the higher the temperature is, the easier of the formation of $CaCO_3$ and $CaSO_4$ scales is. Traditional chelating agents and naturally occurring polymers are also limited because they are unstable in high-temperature conditions and a higher minimum inhibitor concentration requirement. Threshold inhibitors are welcomed to form a mass of coordinative bonds with organic ions after adsorption at an active crystal growing point related to the binding energy; this retards the continuous nucleation growth along a certain direction and thus slows down the crystal growth rate.[14,21,22] As a result, the morphology, pattern, and size of the scales are greatly changed, and a loosened scale layer is formed and then washed away by the flowing line.[15]

In recent years, double-hydrophilic block polymers have attracted great interest from polymer researchers for their advantageous structures. Because each block can be designed in an optimum way for its desired use, different functions are separated within one molecule.[23] Poly(ethylene glycol) (PEG)/poly (ethylene oxide) (PEO), allyl poly(ethylene glycol) APEG/allyl poly(ethylene oxide) APEO and methoxy poly(ethylene glycol) (CH_3—PEG—OH) are the main raw materials in the hydrophilic polyether segment. Many of their derivatives have been reported as novel surfactants and crystal modifiers, including PEO-*block*-polyethyleneimine (PEI) (—SO_3H/—COOH/—PO_3H_2), PEO-*block*- poly(2-vinylpyridine) (P2VP), PEO-*block*-PMAA (aspartic acid (Asp)/—PO_3H_2), PEO-*block*-poly(methyl oxazoline) (PMOX), PEO-*block*-poly(methyl vinyl ether) (PMVE), PEO-*block*-poly(ethylenediaminetetraacetic acid) (PEDTA), PEO-*block*-PEI-$COC_{11}H_{23}(CH_2COOH)_n$, CH_3—PEG-*block*-poly (N-carboxymethyl)ethyleneimine (PEIPA), PEG-*block*-EDTA (ethylene diamine tetraacetic acid), allylpolyethoxy carboxylate (APEC)/acrylic acid (AA), APEG–polyglycerol (PG)(—COOH)/PAA, and so on.[22–31] From this point, in this study, we synthesized a novel PEG-based double-hydrophilic and environmentally friendly copolymer polyethylene glycol double-ester of maleic anhydride/acrylic acid named PEGDMA-AA, whose structure is still linear but also has some differences from traditional chelating linear polymers, in which the PEG segments are incorporated into the polymer structure. The polymer hydrophilic block PAA is used as an efficient builder for calcium binding, as the hydrophilic PEG block just promotes dissolution in water but does not react with the dissolved ions (or just weakly interacts with the ions).[29,32–34] In addition to this, the raw materials used for synthesis are economically efficient, and the copolymer is phosphor-free and nitrogen-free and has a superior calcium tolerance, even in wicked conditions. PEGDMA/AA was also synthesized for the first time in our laboratory, and the inhibiting power satisfied the principle for application potential in industrial water systems.

EXPERIMENTAL

Materials

The PEG (PEG_n) used in the experiment was analytical grade and had an average molecular weight (MW) of 200, 400, and 600 (the corresponding polymerization degree f = 3, 8, and 12). The AA, maleic anhydride, and ammonium persulfate (APS) we used were analytically pure grade and were supplied by Zhongdong Chemical Reagent Co., Ltd. (Nanjing, Jiangsu, People's Republic of China). The commercial inhibitors of PAA (MW = 1800), HPMA (MW = 600), PESA (MW = 1500), HEDP (MW = 206), and PBTC (MW = 270) were technical grade and were supplied by Jiangsu Jianghai Chemical Co., Ltd. (Changzhou, Jiangsu, People's Republic of China). APEC/AA and APEG–PG/AA were synthesized by Du and Ling in our laboratory. Distilled water was used in all of the studies.

Characterization

^{1}H-NMR spectra were recorded on a Mercury VX-500 spectrometer (Bruker AMX500) with a tetramethylsilane internal reference and deuterated dimethyl sulfoxide as the solvent. The MWs and MW polydispersities were determined by gel permeation chromatography (GPC; Waters-2410, calibrated with PEG standards) with water as the eluent at a flow rate of 1.0 mL/min. The shapes of $CaCO_3$ and $CaSO_4$ were observed with scanning electron microscopy (SEM; S-3400N, HITECH, Japan) and transmission electron microscopy (TEM; JEM-2100SX, Japan). The X-ray diffraction (XRD) patterns were measured on a Rigaku D/max 2400 X-ray powder diffractometer with Cu Kα radiation (λ = 1.5406, 40 kV, 120 mA).

Synthesis of the Macromonomer of PEG_nDMA

Transformation into the carboxylate-terminated double-hydrophilic block polymer PEG_nDMA was performed by the esterification of terminal two hydroxyl groups in PEG_n subjected to maleic anhydride with a molar ratio of 1:2 in high yields exceeding 99%, as shown in Scheme 1. The obtained

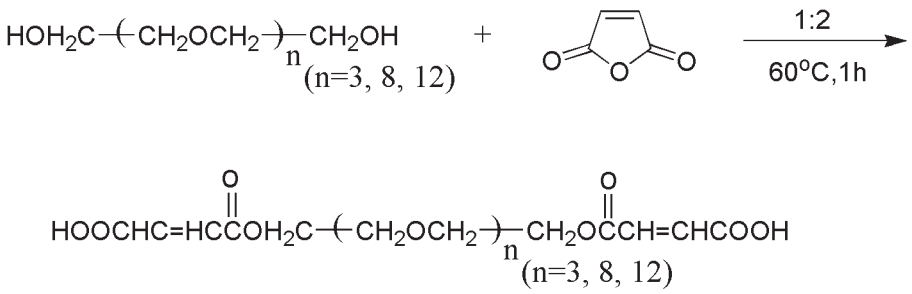

Scheme 1. Synthesis of PEG$_n$DMA.

macromonomers were a dark wine color and posed a higher viscosity compared with PEG$_n$.

Synthesis of the PEG-Based Copolymer PEG$_n$DMA/AA

A six-necked, round-bottomed flask, equipped with a thermometer, a mechanical agitator, and a reflux condensing tube was charged with 5 mL of deionized water and 6 g of PEG$_n$DMA and then heated to 80°C with fierce stirring. Nitrogen gas was filtered into the reaction unit to cast away oxygen gas to protect the initiator from being oxidized. Both AA and APS were diluted before they were cast into the reaction unit, as a higher concentration of substrate may be out of control. A certain amount of AA in 20 mL of deionized water and the initiator APS solution in 20 mL of deionized water were injected into the flask at constant flow rates over a certain period, respectively. After that, the temperature was heated to 90°C and maintained for 2.5 h to finally obtain the faint yellow liquid with an approximately 21% solid content. A different polymerization degree PEG$_n$DMA were used for the synthesis with AA. The procedure for the synthesis of PEGD$_8$MA–AA is given in Scheme 2.

Static Scale Inhibition Methods

All deposit experiments were carried out in triplicate, and all of the inhibitor dosages given were based on a dry inhibitor. The analytical reagent, A-grade glassware, and deionized water were used throughout. The $CaCO_3$ scale was deposited with a mixture of certain amounts of $CaCl_2$ and $NaHCO_3$ solutions, according to the national standard of People's Republic of China concerning the code for the design of industrial circulating cooling-water treatments (GB/T 16632-2008). The final concentrations of Ca^{2+} and HCO_3^- were 240 and 732 mg/L, respectively, with the solution pH 9 adjusted by a borax buffer solution. Investigation with inhibitors and without inhibitors were all carried out. To prevent the concentration of the solution by evaporation, especially at a high temperature, we condensed the vapor by means of a cooler. The deposition of these $CaCO_3$ supersaturated solutions was filtered with filter paper after these solutions were incubated at 80°C for 10 h. The Ca^{2+}-ion concentration in the residual filtered fluid was analyzed by an ethylene diamine tetraacetic acid disodium salt (EATA) complexometric titration method according to the national standard of People's Republic of China concerning the code for the design of industrial circulating cooling-water treatment (GB/T 15452-2009). At the end point of titration, the color of the solution changed from purple red into dark blue with a calcon–carboxylic acid indicator. The copolymer inhibition efficiency for $CaCO_3$ was calculated with the following equation:

$$\text{Inhibition efficiency}\,(\%) = ([Ca^{2+}]_{\text{final}} - [Ca^{2+}]_{\text{blank}})/([Ca^{2+}]_{\text{initial}} - [Ca^{2+}]_{\text{blank}})$$

where $[Ca^{2+}]_{\text{final}}$ and $[Ca^{2+}]_{\text{blank}}$ are the concentrations of Ca^{2+} ions in the filtrate liquor in the presence of inhibitor and without the presence of inhibitor, respectively, after the $CaCO_3$ supersaturated solutions were heated at 80°C for 10 h and $[Ca^{2+}]_{\text{initial}}$ is the maximum concentration of Ca^{2+} ions at the beginning of the scale tests. Commercial-scale inhibitors with different molecular structures and MWs, such as PAA, HPMA, PBTC, and PESA, were also tested to obtain a comparison of different inhibition efficiencies.

The procedure of the $CaSO_4$ inhibition test was similar to the $CaCO_3$ experiments according to the national standard of People's Republic of China concerning the code for the design of industrial oil field–water treatments (SY/T 5673-93). $CaCl_2$ and $NaHCO_3$ solutions were substituted by $CaCl_2$ and Na_2SO_4 mixed solutions with the final scale solution concentration of 6800 and 7100 mg/L. The pH of the $CaSO_4$ solutions were adjusted to 7.0 with hydrochloric acid or sodium hydroxide. After heat preservation at 70°C for 6 h, the determination of Ca^{2+} was done by exactly same process.

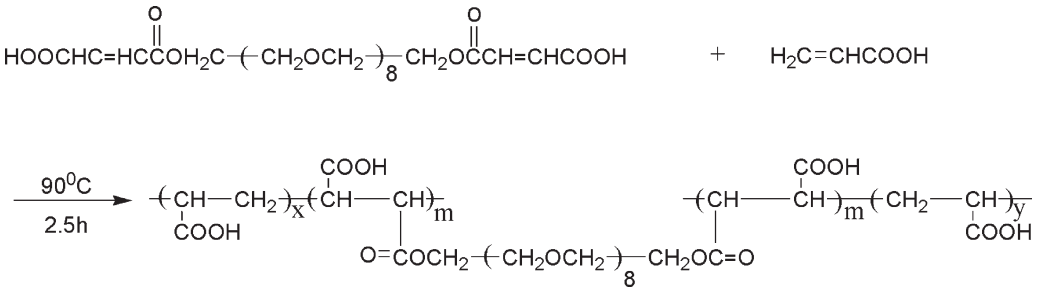

Scheme 2. Synthesis of PEG$_8$DMA/AA.

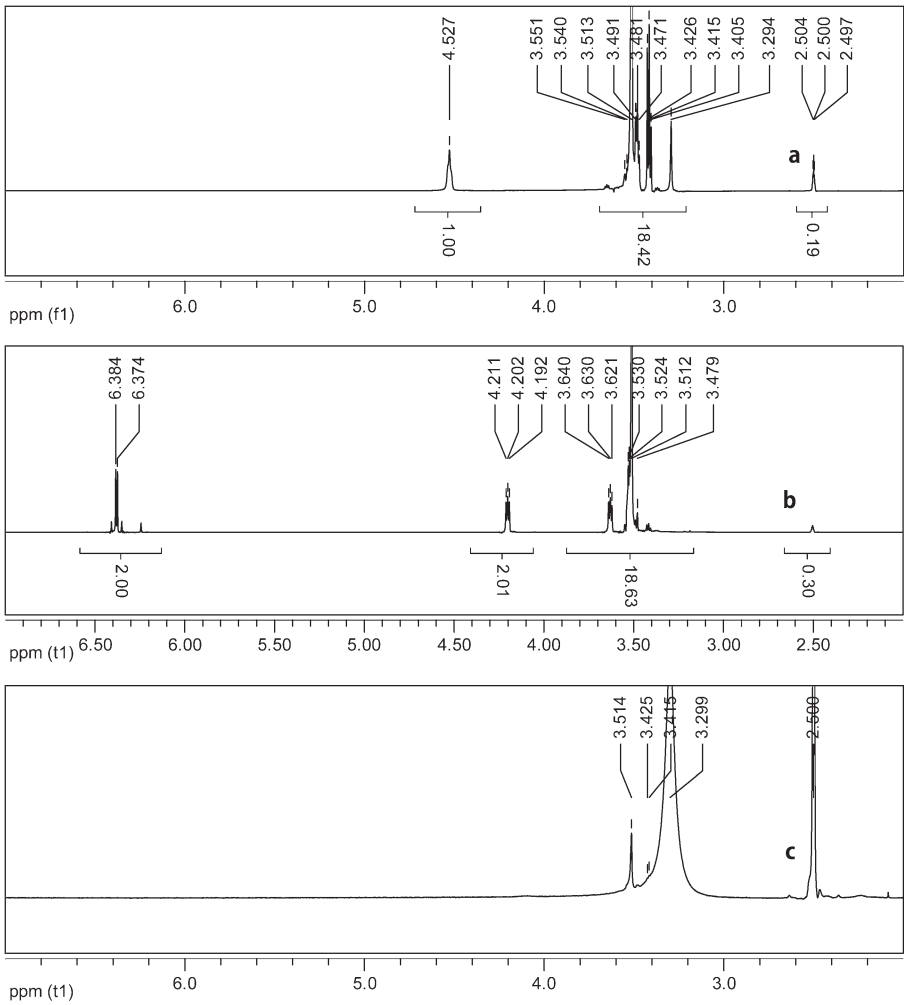

Figure 1. ^{1}H-NMR spectra of (a) PEG, (b) PEG_8DMA, and (c) PEG_8DMA/AA.

RESULTS AND DISCUSSION

^{1}H-NMR Spectra of PEG_8, PEG_8DMA, and PEG_8DMA/AA

The ^{1}H-NMR spectra of PEG_8, PEG_8DMA, and PEG_8DMA/AA are presented in Figure 1.

H-NMR (δ, ppm): PEG_8 [$(CD_3)_2SO$]: 2.50 [solvent residual peak of $(CD_3)_2SO$], 3.29–3.55 (—OCH_2CH_2—, ether groups), 4.53 (—OH, active hydrogen in PEG_8) [Figure 1(a)]; PEG_8DMA [$(CD_3)_2SO$]: 3.48–3.64 (—OCH_2CH_2—, ether groups), 4.19–4.21 (—CH_2OC═O, protons close neighbor to carbonyl group), 6.37 (—CH═CH—, ethylene group) [Figure 1(b)].

It was obvious that the hydroxyl group (—OH, δ = 4.53 ppm) in Figure 1(a) disappeared completely, and the —CH═CH— protons were obvious at δ = 6.37 ppm, as shown in Figure 1(b). Meanwhile, the peaks at δ = 4.20 ppm proved the existence of carbonyl groups. All of these suggested that the —OH groups in PEG_8 were entirely transformed into —OC(═O)CH═CHCOOH and PEG_8DMA was synthesized successfully.

PEG_8DMA/AA [$(CD_3)_2SO$, δ, ppm]: 2.50 [solvent residual peak of $(CD_3)_2SO$], 3.30–3.51 (—OCH_2CH_2—, ether groups).

The double-bond adsorption peaks at δ = 6.37 ppm in Figure 1(b) completely disappeared in Figure 1(c); we concluded that free-radical polymerization between PEG_8DMA and AA occurred.

GPC Testing of the PEG_8DMA/AA Polymer MW Distribution

The PEG_8DMA/AA weight distribution was investigated with GPC with the 1.0 mL/min run flow rate. It was obvious from Figure 2 that PEG_8DMA/AA was not very polydisperse; the MW spread between the interval of 10×10^3 and 10×10^4. This was achieved by the control of the drop rate of the initiator, monomer solutions, and timely chain termination. The weight-average molecular weight (M_w) was 40,876, whereas the number-average molecular weight (M_n) was 29,930; thus, we obtained a polydispersity index (PD) of 1.3657 (PD = M_w/M_n). Molar mass at the maximum peak (M_p), viscosity-average molecular weight (M_v), and the z-average molecular weight (M_z) were also obtained in the calculated report.

Influence of the Dosage and PEG_nDMA Polymerization Degree on the Scale Inhibition

The relationship between the inhibitor dosage and the inhibition capacity toward the $CaCO_3$ and $CaSO_4$ scales was investigated and is presented in Table I, as the relationship between the polymerization degrees of PEG_nDMA and the antiscaling ability. It was obvious that when the dosage was at a level of 2

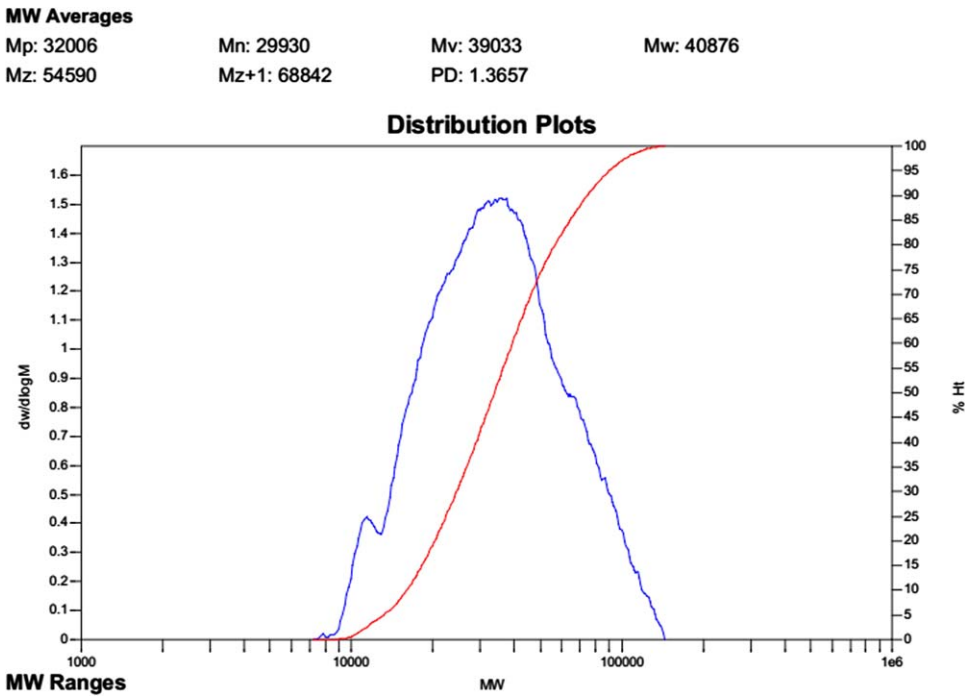

Figure 2. GPC results for the MW distribution of PEG_8DMA/AA. [Color figure can be viewed in the online issue, which is available at wileyonlinelibrary.com.]

mg/L, PEG_nDMA/AA had a lower calcium tolerance, with 14.3, 18.9, and 11.2% $CaCO_3$ inhibition efficiencies for PEG_3DMA/AA, PEG_8DMA/AA, and $PEG_{12}DMA/AA$, respectively. As the dosage was gradually increased, the inhibition performance improved substantially, and the maximum inhibitory power was obtained at a certain dosage, called the *threshold value*. The threshold dosage was the same at 12 mg/L for $CaCO_3$, and the maximum inhibition efficiency reached 65.1, 89, and 54.7%, respectively. A similar tendency was reported in earlier studies about polymeric threshold inhibitors.[31] What should be noted is that the PEG_nDMA polymerization degree also had a great influence on the scale function. Compared with PEG_3DMA/AA and $PEG_{12}DMA/AA$, PEG_8DMA/AA exhibited much better inhibition performance; the reason may be that when the degree of polymerization was lower, the ratio of $-OCH_2CH_2/-COOH$ groups is rather small. Even though there were abundant chelating —COOH groups, after chelating with calcium ions, it was much easier to form insoluble polymer–calcium depositions because of the wretched content of water-soluble polyether ($-OCH_2CH_2$) chain segments; this could enhance the solubility of polymer–calcium in water. For parallel reasons, too many $-OCH_2CH_2$ groups in the polymer molecule lead to a higher ratio of $-OCH_2CH_2$ groups to —COOH groups. In this case, the —COOH chelation group was finite so as not to combine with a mass of scale particles; thus, the inhibition efficiency was lower, too. The influence of the polymerization of PEG on scale inhibition was also studied in our laboratory before.[35]

The effect of the dosage of PEG_nDMA/AA on the $CaSO_4$ scale was analogous to the $CaCO_3$ scale inhibition. Below the threshold dosage value, the relationship was positively correlated, and

Table I. Influence of the Dosage and Polymerization Degree of PEG_nDMA on the Inhibition Tests of $CaCO_3$ and $CaSO_4$

	$CaCO_3$ inhibition (%)				$CaSO_4$ inhibition (%)		
PEG_nDMA/AA dosage (mg/L)	PEG_3DMA/AA	PEG_8DMA/AA	$PEG_{12}DMA/AA$	PEG_nDMA/AA dosage (mg/L)	PEG_3DMA/AA	PEG_8DMA/AA	$PEG_{12}DMA/AA$
2	14.3	18.9	11.2	1	32.1	59.2	45.6
4	44.6	68.0	25.2	2	77.8	89.3	57.8
6	58.5	81.6	35.8	3	98.3	98.8	69.3
8	62.9	87.5	44.7	4	98.2	98.9	75.2
10	63.9	88.4	52.1	5	98.6	98.9	88.6
12	65.1	89.0	54.7	6	98.5	98.7	98.5
14	65.1	89.2	54.9	7	98.5	98.7	98.5
16	65.1	89.3	54.9	8	98.6	98.9	98.6

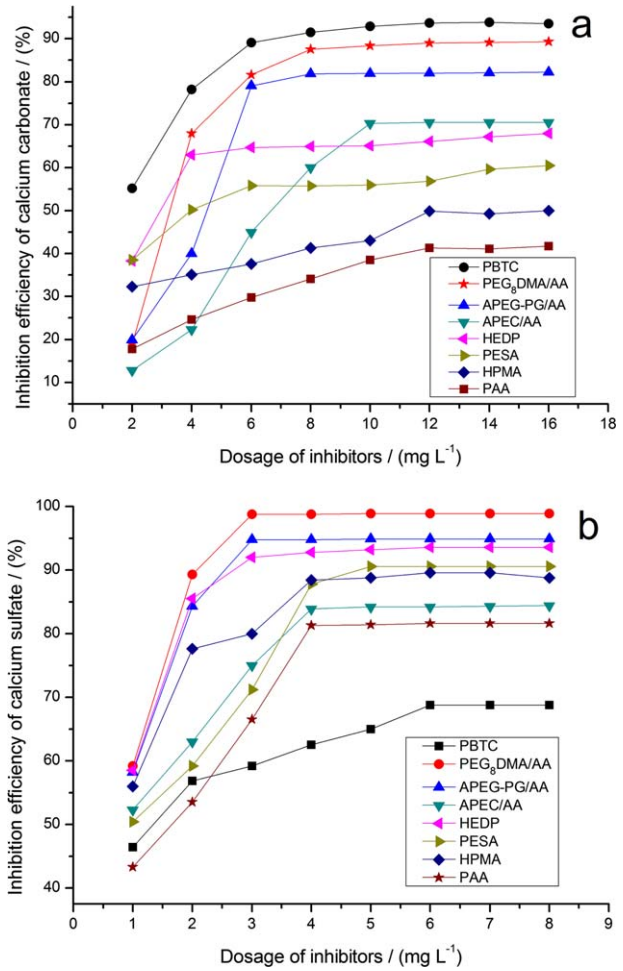

Figure 3. Comparison of inhibition efficiency for (a) $CaCO_3$ and (b) $CaSO_4$. [Color figure can be viewed in the online issue, which is available at wileyonlinelibrary.com.]

the inhibition efficiency showed almost no change once it reached the threshold value. Obviously, no matter how much bigger or smaller of polymerization degree of PEG_nDMA was, its copolymers with AA (PEG_nDMA/AA) all achieved an approximately equivalent inhibition efficiency (98.7%), but it is worth mentioning that the threshold dosage was different (3 mg/L for PEG_3DMA/AA and PEG_8DMA/AA and 6 mg/L for $PEG_{12}DMA/AA$, diversely). In an analysis of the previous results, when the polymerization degree of PEG was 8 ($n = 8$), the best performance was obtained, and we concluded that PEG in the PEG_nDMA/AA matrix played a significant role in the inhibition of $CaCO_3$ and $CaSO_4$.

Comparison of Inhibition Efficiency

To gain a better understanding of the stand or fall of the PEG_8DMA/AA inhibition power, the effects of PEG_8DMA/AA on the $CaCO_3$ and $CaSO_4$ scale inhibition was compared with currently frequently used phosphorus antiscalants PBTC, HEDP, nonphosphorus antiscalants PESA, HPMA, PAA, and polyether antiscalants APEG–PG/AA, APEC/AA synthesized by Ling and Du and consisting of different functional groups [i.e., —COOH, $—PO(OH)_2$, —OH, $—OCH_2CH_2$]. The compared results are shown in Figure 3.

From Figure 3(a), the most outstanding inhibitor for $CaCO_3$ was PBTC; this is also the most used water treatment in industrial water systems. Except for PBTC, PEG_8DMA/AA displayed superior control power compared to other inhibitors in preventing or retarding the growth of $CaCO_3$, with a more little inefficiency than PBTC. However, PBTC contains phosphorus element in its structure, which is not desirable in water additives, whereas PEG_8DMA/AA had only three elements, C, H, and O and was environment friendly. The order of controllability on $CaCO_3$ was as follows: PBTC > PEG_8DMA/AA > APEG–PG/AA > APEC/AA > HEDP > PESA > HPMA > PAA. The earlier synthesized APEG–PG/AA (linear dendritic polymer) and APEC/AA in our laboratory exhibited relatively nice properties, but the raw material glycidol, used for synthesis of APEG–PG/AA, is costly, and the chloroacetic acid ($ClCH_2COOH$) used for synthesis of APEC is controlled because its hypertoxic; both of these have limited applications in industrial fields. Analysing the comparison results of PESA, HPMA, PAA, and APEC/AA, consisting of carboxyl (—COOH) functional groups and possessing a similar molecular structure to PEG_8DMA/AA, we came to the following three conclusions:

1. The PEG segments in PEG_8DMA/AA played an important role during the crystal growth process and the reaction between Ca^{2+} ions and —COOH and $—OCH_2CH_2$ functional groups; this results in the formation of polyion complex micelles and the outer PEG chain segments surrounding the core of the polyion complex in water.
2. A double-hydrophilic block copolymer was better than inhibitors, such as PAA and HPMA, which only had one hydrophilic function.
3. The macromonomer PEG_8DMA had two double bonds (—C═C—) in its structure; this made it easier to produce high-molecular-weight polymer with other monomers (the best MW for inhibition was 10^3–10^4 g/mol). The chemical composition of inhibitors affected the performance deeply.

Figure 3(b) shows the outstanding ability than other commonly used antiscalants on the $CaSO_4$ scale to distribute the germination and aggregation into big particles. The capability was as follows: PEG_8DMA/AA > APEG–PG/AA > HEDP > PESA > HPMA > APEC/AA > PAA > PBTC. The inhibitors of PEG_8DMA/AA, APEG–PG/AA, and APEC/AA had threshold dosages of 3, 3, and 4 mg/L, and the maximum inhibitory powers were different: 98.9, 94.7, and 84.4%, respectively. The inhibition efficiency also remained constant after it attained the ultimate inhibition efficiency values for HEDP, PESA, HPMA, PAA, and PBTC (93.6, 90.6, 88.8, 81.6, and 68.8%, respectively) at dosage levels of 3, 5, 4, 4, and 6 mg/L. It is worth noting that the most effective $CaCO_3$ water additive, PBTC, had a relatively poor antiscaling function on $CaSO_4$; this suggested that function of some of the inhibitors were not perfect. Meanwhile, PBTC had phosphorus in its structure, and this is not desirable in water additives. In this study, the newly synthesized PEG-based PEG_8DMA/AA was a versatile, nonphosphorus, and environmentally friendly scale inhibitor, not only for $CaCO_3$ but also for $CaSO_4$, with the potential to be applied in industrial water systems, not only to solve the water eutrophication problems caused by phosphorus but because of its economic efficiency.

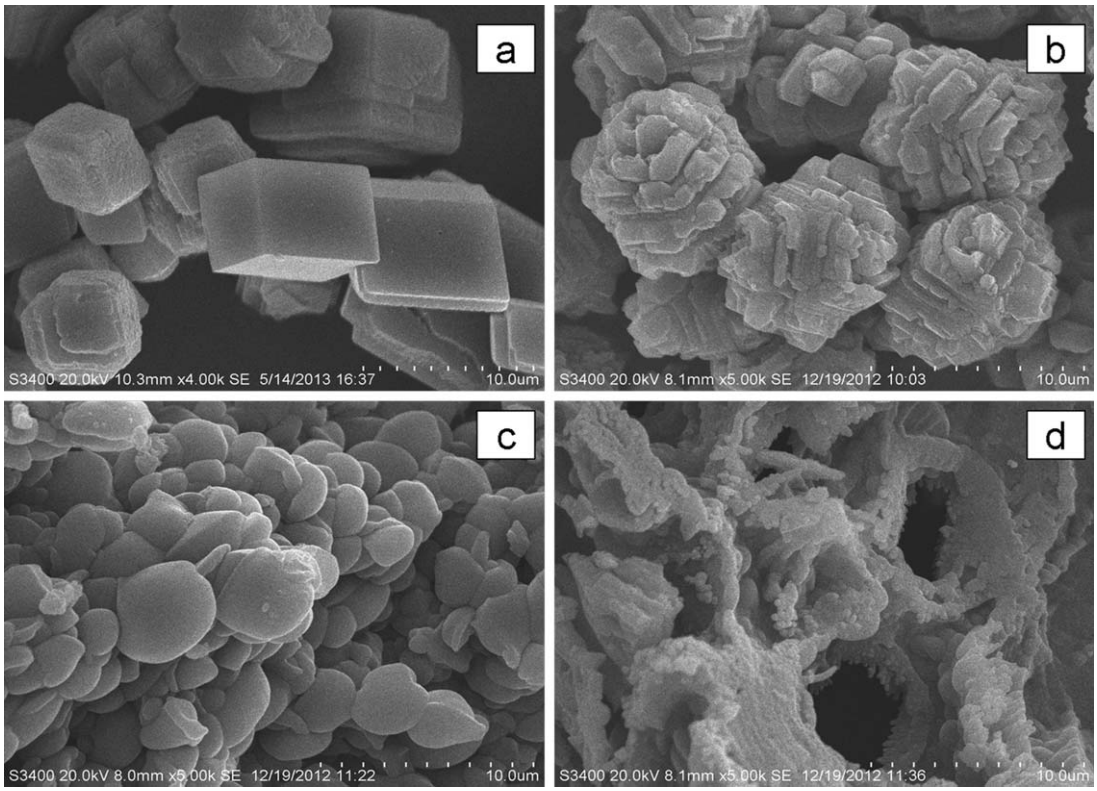

Figure 4. SEM images of the $CaCO_3$ scales (a) in the absence of an inhibitor and (b–d) in the presence of 2, 4, and 8 mg/L PEG_8DMA/AA, respectively.

Characterization of the $CaCO_3$ and $CaSO_4$ Scales

The presence of antiscalants affects the morphology, size, and pattern of calcium crystals significantly. Figure 4 shows the SEM photographs of $CaCO_3$ with and without the PEG_8DMA/AA.

It was obvious that the amount of the inhibitor PEG_8DMA/AA had a great influence on the $CaCO_3$ crystal morphology and size. Both the morphology and size varied greatly; the reason was that polymeric matrix/template controlled the modification of the developing crystal through epitaxy.[32] In the absence of PEG_8DMA/AA, the formed crystal had the regular shape of a rhombohedron or cube, and the particle size was about 10 μm [Figure 4(a)]. However, in the presence of PEG_8DMA/AA, even at a rather low dosage of 2 mg/L, the regular appearance was peeled into a flowerlike shape, and the size was decreased to 7–8 μm [Figure 4(b)]. The higher the concentration of PEG_8DMA/AA was, the greater the change was; flaky-shaped crystals [Figure 4(c)] and inner hollow crystals [Figure 4(d)] were obtained, respectively, with much smaller size dimensions. The reduction of rust particles (major nucleating sites for scale crystals) in artificial water may help to reduce scale deposition. Except for that, a relative narrowing of the size distribution of the particles was observed visually; in other words, the crystal lengths were restricted as well.

The SEM photographs for the $CaSO_4$ scales are shown in Figure 5. Regular rod-shaped and tubular $CaSO_4$ crystals exhibiting monoclinic symmetry are depicted in Figure 5(a) in the absence of inhibitor, with an unbroken regular smooth surface. However, in the presence of even 0.5 mg/L PEG_8DMA/AA, the integrated structure was violated, and it lost its glossy surface appearance and was relatively rough [Figure 5(b)]. This indicated that the dosage of PEG_8DMA/AA had a profound effect on the modification the morphology of the $CaSO_4$ crystals. With the continued increase in the PEG_8DMA/AA dosage, the crystal surface was damaged more seriously as a flaky crystal or tabular crystal shape [Figure 5(c)] began to emerge from the $CaSO_4$ saturated solution at a dosage level of 1.5 mg/L PEG_8DMA/AA; this proved that bigger changes took place in the inner space of the $CaSO_4$ crystal. The much destroyed loose-knit particles [Figure 5(d)], which had a much smaller size and could be easily washed away by running water, appeared with a dosage of 2 mg/L PEG_8DMA/AA. This could be explained as the combined action of chelating —COOH groups and water-soluble PEG segments. PEG_8DMA/AA was able to enclose the grain and retard the outgrowth of calcium salts crystals, including the lattice distortion effect.

The $CaCO_3$ precipitated phases were also identified by XRD, and the corresponding spectra are given out in Figure 6. As it is well known, $CaCO_3$ exists in three types of crystal forms: calcite, aragonite, and vaterite, among which calcite and vaterite are the most and least thermodynamically stable, respectively. It is traditionally recognized that vaterite crystals are the initial phase form in $CaCO_3$ saturation solutions, and they can transform into calcite spontaneously if there is no interference, but

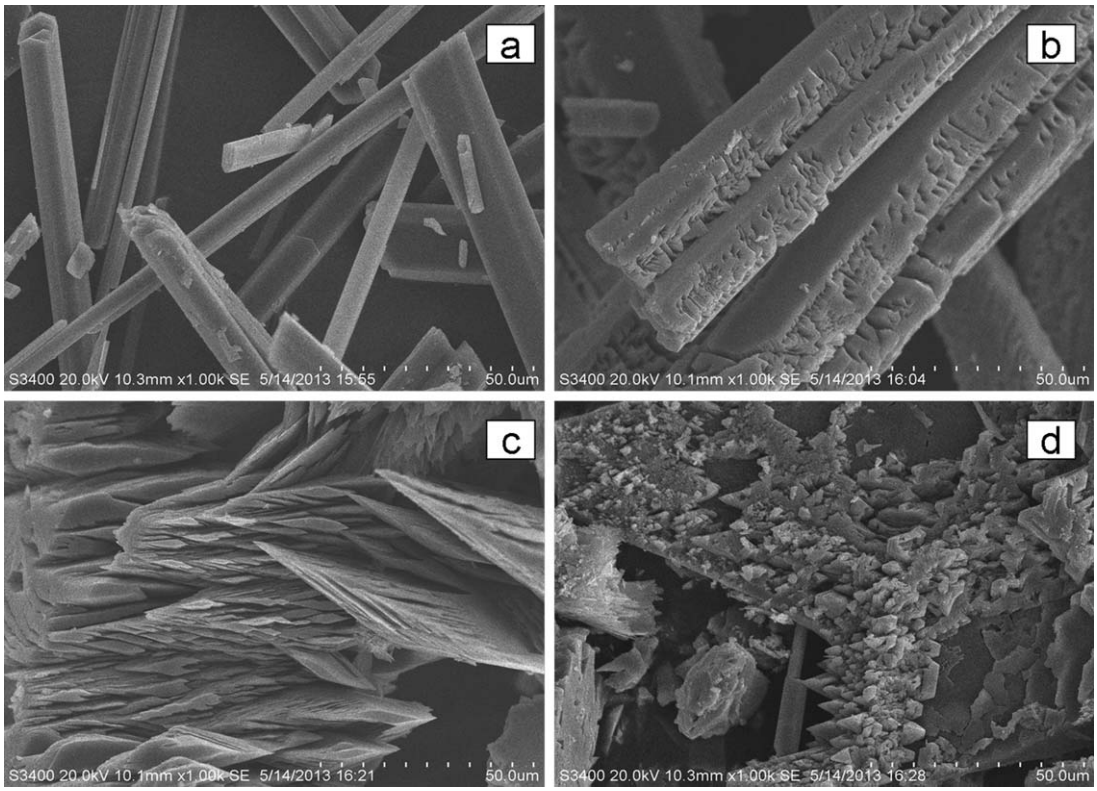

Figure 5. SEM images of the $CaSO_4$ scales (a) in the absence of an inhibitor and (b–d) in the presence of 0.5, 1, and 2 mg/L PEG_8DMA/AA, respectively.

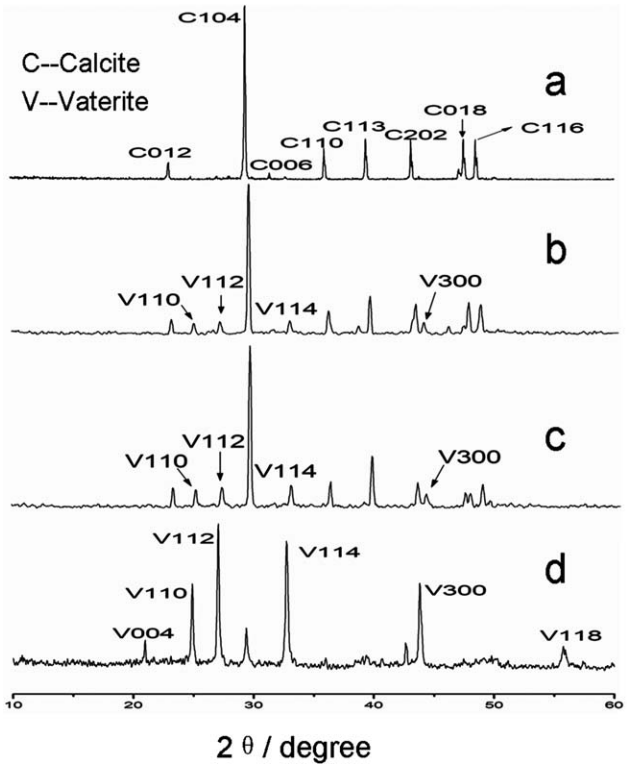

Figure 6. XRD pattern of the $CaCO_3$ crystals (a) in the absence of an inhibitor and (b–d) in the presence of 2, 4, and 8 mg/L PEG_8DMA/AA, respectively.

under certain conditions, such as with pH changes and injection of inhibitors, it also can be stabilized in water solutions.[36] In the absence of an antiscalant [Figure 6(a)], calcite was the only crystal formed, and the reflection peaks appeared at (012), (104), (006), (110), (113), (202), (018), and (116). In the presence of 2 or 4 mg/L PEG_8DMA/AA, there were (110), (112), (114), and (300) weak peaks, which corresponded to vaterite [Figure 6(b,c)], with the exception of calcite peaks. As the use of PEG_8DMA/AA increased to 8 mg/L PEG_8DMA/AA, vaterite crystals became the relatively dominant crystal form, and also, new vaterite peaks appeared at (004) and (118) [Figure 6(d)] compared with the previous two spectra. All of this suggests that the $CaCO_3$ scales were a mixture of calcite and vaterite crystals with inhibitors. Meanwhile, three apparent distinctions were observed from the spectra:

1. The peaks for calcite at (104) and (202) became weaker and weaker, whereas those at (012), (110), 113), (018), and (116) were weakened to disappearance in the spectra.
2. Vaterite peaks at (110), (112), (114), and (300) varied from weaker to strongly intense with increasing dose of PEG_8DMA/AA.
3. Among the investigated results, only in the 8 mg/L PEG_8DMA/AA did there exist (004) and (118) vaterite peaks.

These results manifest that not only the $CaCO_3$ crystal size and shape changed but also that the crystals forms altered to an extent.

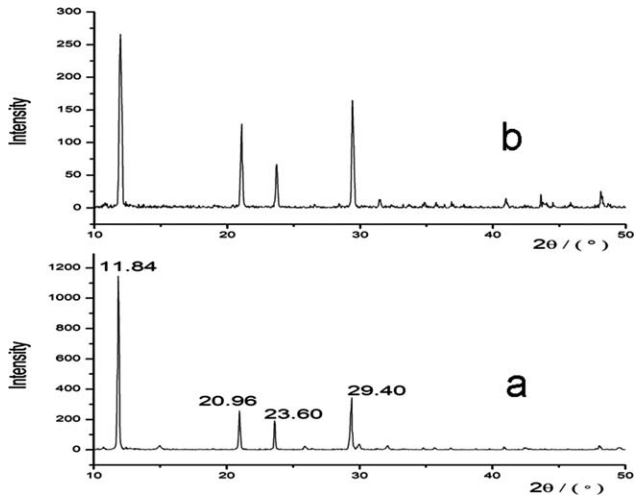

Figure 7. XRD pattern of the $CaSO_4$ (a) in the absence of an inhibitor and (b) in the presence of PEG_8DMA/AA.

Figure 7 reveals the $CaSO_4$ crystal X-ray pattern with and without the presence of PEG_8DMA/AA. The interplanar crystal spacing (d) and angle of intersection (θ) values conformed to the $CaSO_4$ dehydrate $CaSO_4{\cdot}2H_2O$, namely gypsum. In both cases, there were reflection peaks in the same angle of intersection (θ) angles but with different intensities. The results indicate that the crystal forms were not altered, despite the enormous change in crystal morphology, but the degree of crystallinity deviated badly.

TEM was used to carry out further detailed research toward $CaCO_3$ and $CaSO_4$ crystals, and the investigation results are shown in Figure 8. As shown in Figure 8(a), integrated symmetrical monoclinic hexahedron calcite crystals were observed once more, as shown in SEM [Figure 4(a)], and in the plugged diffraction pattern, there existed as a perfect monocrystal in accordance with the XRD results without inhibitor. In the presence of PEG_8DMA/AA, the $CaCO_3$ scale lost its unabridged structure, and the decrescent particles were distributed randomly. The asystematic orbicular or circular pattern confirmed the existence of both the calcite and vaterite crystals in Figure 8(b). The cracked segments were aggregations of smaller microcrystals, and the diaphragm and particle diameters were all on a nanometer order of magnitude.

Figure 8(c,d) shows images of $CaSO_4$ crystal growth in the absence and presence of PEG_8DMA/AA. It was obvious that great changes occurred for the $CaSO_4$ crystals as the entire long clubbed crystal (ca. 3 μm) was divided into a mass of smaller segments (100–300 nm). It is worth noting that the particles modified by PEG_8DMA/AA were lacunose and inner-loosened. The achieved more-or-less-uniform rings shown in Figure 8(d) compared with the diffraction pattern without indication of the underlying powder rings shown in Figure 8(c) demonstrated randomly oriented particles in $CaSO_4$ water solutions.

In sum, characterization by means of SEM, XRD, and TEM richly manifests the influence of PEG_8DMA/AA on the crystal size, pattern, shape, and morphology of the calcium scales. They

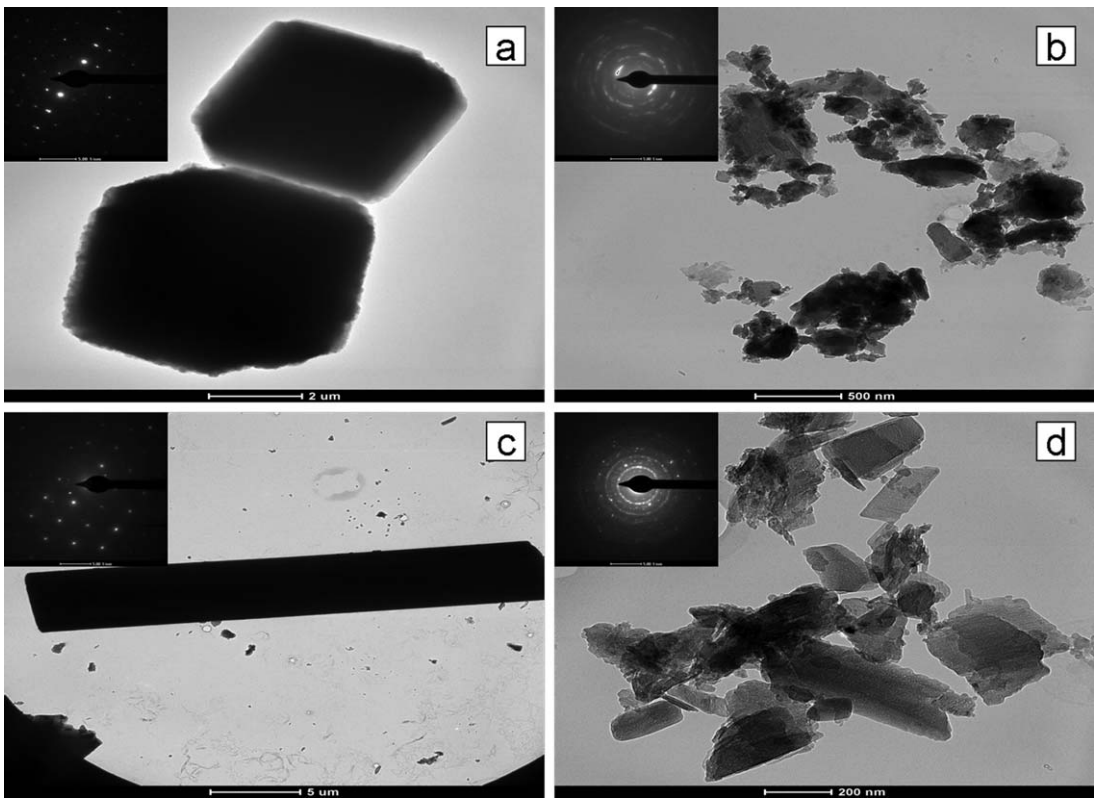

Figure 8. TEM micrograph and diffraction patterns: (a) $CaCO_3$ crystals in the absence of an inhibitor, (b) $CaCO_3$ crystals in the presence of PEG_8DMA/AA, (c) $CaSO_4$ crystals in the absence of an inhibitor, and (d) $CaSO_4$ crystals in the presence of PEG_8DMA/AA.

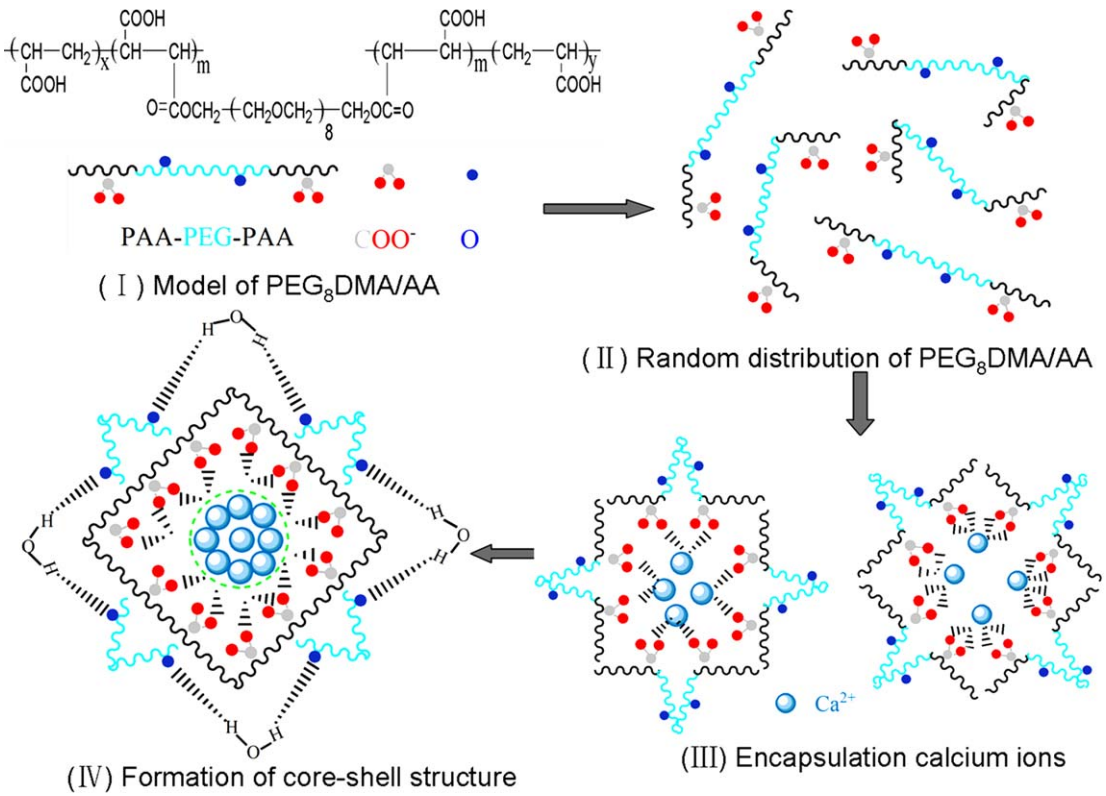

Figure 9. Schematic diagrams of PEG_8DMA/AA inhibition on calcium scales: chelating solubilization function. [Color figure can be viewed in the online issue, which is available at wileyonlinelibrary.com.]

have tremendous potential to be used as crystal modifiers for the mineralization of scales in the water treatment field.

Mechanisms of the PEG_8DMA/AA Inhibition of Calcium Scales

The scale process of microsolubility salts ($CaCO_3$, $CaSO_4$, etc.) in cooling-water systems is just the process of crystal formation, which follows the steps of the attainment of supersaturated solutions, generation of crystal nucleus, and crystal nucleus growth into crystals.[37] The induction period of nucleation from supersaturated solutions was significantly decreased by prodigious orders of magnitude with the addition of antiscalants; this destroyed the crystallization process and restrained scale precipitation. The mechanisms of PEG_8DMA/AA inhibition were supposed to be

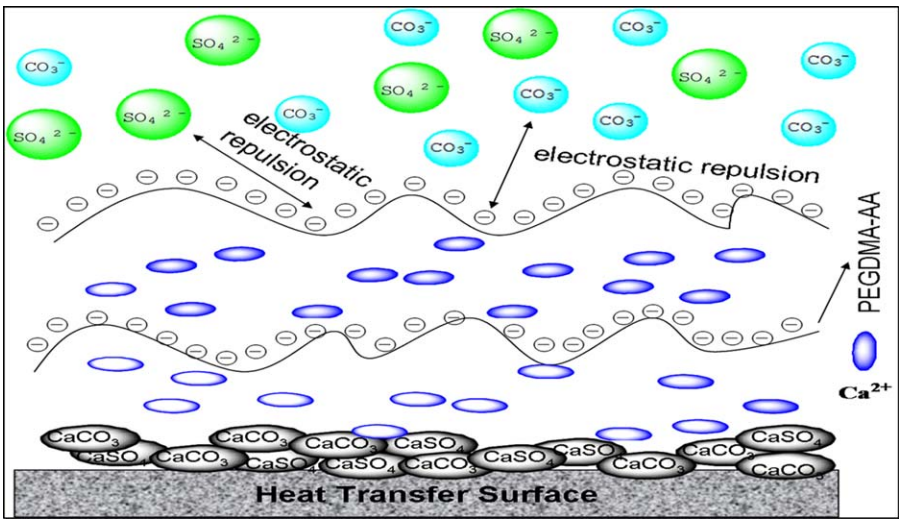

Figure 10. Schematic diagrams of PEG_8DMA/AA inhibition on calcium scales: combined effect of a multilayer type of adsorption on the scale surface and electrostatic repulsion function. [Color figure can be viewed in the online issue, which is available at wileyonlinelibrary.com.]

chelating solubilization, as depicted in Figure 9, and the joint action of multilayer types of adsorption on the scale surface and electrostatic repulsion function, as shown in Figure 10.

Figure 9(a) gives the main inhibition mechanism in a saturated solution containing a great amount of scale nucleation ions but not at the scale surface. PEG_8DMA/AA was a well-defined, double-hydrophilic block copolymer, as depicted in Figure 9(I). One of the blocks was PAA, and another block was PEG. Both of them were hydrophilic chain segments. Because of the rotation of carbon–carbon bonds, the molecules provided favorable flexibility and existed in different molecular forms, all of which were distribute randomly in water, as shown in Figure 9(II). Once confronted with Ca^{2+} ions, the carboxyl groups (—COOH) in PEG_8DMA/AA recognized and encapsulated or reacted with them to spontaneously form $PEG_8DMA/AA–Ca^{2+}$ complexes. The complexation did not proceed on the basis of the stoichiometric ratio. There were two encapsulation methods: one method was that adjacent —COOH groups in the inside of one molecule chelated with Ca^{2+} ions, and another method was that adjacent —COOH in two molecules functioned with Ca^{2+} ions, just as presented in Figure 9(III). At the same time, the PAA parts twisted with each other together with the combined Ca^{2+} ions encapsulated inside and formed cores in water solution. The surrounding water-compatible PEG chain segments ($—OCH_2CH_2$) formed hydrogen bonds voluntarily and enhanced the water solubility of the formed $PEG_8DMA/AA–Ca^{2+}$ complexes. In addition to that, J. Orth etc al.[34] reported the steric screening effect of PEG blocks in a simple model for modified nucleation and crystal growth. The self-assembly core–shell structure is given in Figure 9(IV). Ca^{2+} ions were wrapped inside; therefore, the calcium scales did not deposit in the presence of PEG_8DMA/AA because of its wonderful dispersability for solid particles.

Another inhibition mechanism is illustrated at the near surface of the generated scales in Figure 10. The growing calcium crystals contained abundant negative ions ($—SO_4^{2-}$, $—CO_3^-$) and positive ions (Ca^{2+}) at their crystal growth surface. The scaling inhibitor molecules posed a strong adsorption capacity after ionization into anionic polymer because of the physical or chemical effect. After the adsorption of PEG_8DMA/AA to Ca^{2+} ions (the crystal active growing point), the microcrystal scales were electronegative, and the increase in mutual electrostatic repulsive force prevented the collision between particles and the aggregation of larger particles with the growing adsorption of PEG_8DMA/AA. Suspended solids did not easily to settle down; thereby, they were dispersed and washed out throughout the fluid. Meanwhile, the $—SO_4^{2-}$ and $—CO_3^-$ ions were excluded from the surface because of electrostatic repulsion, and the conditional or environmental crystal formation was broken; this prevented the proceeding crystallizing process. PEG_8DMA/AA contained many $—COO^-$ groups in its molecules; this guaranteed the source of negative ions, so that the crystal growth processing was almost ruined completely. The great amounts of PEG_8DMA/AA at the scale surface formed a dense adsorption layer with electronegative $—COO^-$ groups, which were able to adsorb calcium ions continuously. The leading result was the formation of a multiadsorption layer, and calcium ions (Ca^{2+}) were dissociated between the layers far away from the negative ions (CO_3^{2-} and SO_4^{2-}). Electrostatic repulsion restrained the mutual collision into $CaCO_3$ or $CaSO_4$ scales. The location of the adsorbed PEG_8DMA/AA at the crystal surface suppressed the crystal growth along a certain direction. Moreover, beyond that, some of the $PEG_8DMA–AA$ may have been implanted or embedded into the inner space of the crystals and consequently resulted in crystal dislocation, lattice distortion, or the formation of hole structures in the scales, as shown in Figure 4(d). Such structures render scales soft and come easily off of pipelines. The incorporated or adsorbed polymer to the particles boosted the promoted binding efficiency and thus enhanced the adsorption ability.[38] The higher the concentration of PEG_8DMA/AA was, the higher the surface binding capability was. This theory was concordant with the SEM and TEM images shown in Figures 4, 5, and 8.

Table II. SEM-EDS of $CaCO_3$ with and without PEG_8DMA/AA

Without PEG_8 DMA/AA	wt %	atom %	With $PEG_8DMA/$ AA	wt %	atom %
C	19.70	29.68	C	27.01	37.96
O	50.13	56.70	O	49.40	52.11
Ca	30.17	13.62	Ca	23.59	9.93

At the same time, the adsorption on $CaCO_3$ scales was further certified by supplementary SEM-EDS (energy dispersive spectrometer), as illustrated in Table II. The C/Ca ratios were 0.65 and 1.14 for weight percentages and 2.18 and 3.82 for atomic percentages. The higher ratio may have been due to the adsorption of PEG_8DMA/AA on the calcium scale surface.

CONCLUSIONS

In this study, a novel double-hydrophilic, PEG-based crystal growth modifier, PEGDMA/AA, was synthesized; this structure was still linear but also had some differences from traditional chelating linear polymers, in which the PEG segment was incorporated into the polymer structure. The scale inhibition behavior of PEGDMA/AA was evaluated by means of the static scale inhibition method. When the polymerization degree of PEG_nDMA was 8 ($n = 8$), the maximum inhibition toward $CaCO_3$ and $CaSO_4$ were 89.0 and 98.8%, respectively, at dosage levels of 12 and 3 mg/L. Comparisons with the other inhibitors were also carried out. The inhibitory power values for $CaCO_3$ were in the following order: PBTC > PEG_8DMA/AA > APEG–PG/AA > APEC/AA > HEDP > PESA > HPMA > PAA, whereas the order was PEG_8DMA/AA > APEG–PG/AA > HEDP > PESA > HPMA > APEC/AA > PAA > PBTC for $CaSO_4$ inhibition.

Characterization of the $CaCO_3$ and $CaSO_4$ scales with SEM and TEM showed that great changes in the size, morphology, and growth rate of the calcium scales took place under the influence of PEG_8DMA/AA. XRD and diffraction patterns further

confirmed the impact of PEG_8DMA/AA as a crystal growth modifier in water solution. The three supposed mechanisms, (1) chelating solubilization, (2) a multilayer type of adsorption on the scale surface, and (3) electrostatic repulsion function, were also described in detail in this article.

ACKNOWLEDGMENTS

This work was supported by the Prospective Joint Research Project of Jiangsu Province (contract grant number BY2012196), the National Natural Science Foundation of China (contract grant number 51077013), Special Funds for Jiangsu Province Scientific and Technological Achievement Projects of China (contract grant number BA2011086), the Program for Training of 333 High-Level Talents of Jiangsu Province of China (contract grant number BRA2010033), and the Scientific Innovation Research Foundation of College Graduates of Jiangsu Province (contract grant number CXLX13-107).

REFERENCES

1. Eusiel, R.-C.; Medardo, S.-G.; José, P.-O. *Appl. Therm. Eng.* **2013**, *50*, 957.
2. Zhang, J. D.; Chen, L.; Zeng, H.; Yan, X. X.; Song, X. N.; Yang, H.; Ye, C. S. *Desalination* **2007**, *214*, 287.
3. Liu, F.; Lu, X. H.; Yang, W.; Lu, J. J.; Zhong, H. Y.; Chang, X.; Zhao, C. C. *Desalination* **2013**, *313*, 18.
4. Andijani, I.; Turgoose, S. *Desalination* **1999**, *123*, 223.
5. Du, K.; Zhou, Y. M.; Wang, L. Q.; Wang, Y. Y. *J. Appl. Polym. Sci.* **2009**, *113*, 1966.
6. Sathiyanarayanan, S.; Syed Azim, S.; Venkatachari, G. *J. Appl. Polym. Sci.* **2008**, *107*, 2224.
7. Tang, Y. M.; Yang, W. Z.; Yin, X. S.; Liu, Y.; Yin, P. W.; Wang, J. T. *Desalination* **2008**, *228*, 55.
8. Moudgil, H. K.; Yasav, S.; Chaudhary, R. S. *J. Appl. Electrochem.* **2009**, *39*, 1339.
9. Xyla, A. G.; Mikroyannidis, J.; Koutsoukos, P. G. *J. Colloid Interface Sci.* **1992**, *153*, 537.
10. Zeng, J. P.; Wang, F. H.; Zhou, C.; Gong, X. D. *Chin. J. Chem. Phys.* **2012**, *25*, 219.
11. Fu, C. E.; Zhou, Y. M.; Liu, G. Q.; Huang, J. Y.; Wu, W. D.; Sun, W. *Int. J. Polym. Mater.* **2012**, *61*, 341.
12. Koelmans, A. A.; Van der Heijde, A.; Knijff, L. M.; Aalderink, R. H. *Water Res.* **2001**, *35*, 3517.
13. Choi, D.-J.; You, S.-J.; Kim, J.-G. *Mater. Sci. Eng.* **2002**, *335*, 228.
14. Kumar, T.; Vishwanatham, S.; Kundu, S. S. *J. Petrol. Sci. Eng.* **2010**, *71*, 1.
15. Shakkthivel, P.; Vasudevan, T. *Desalination* **2006**, *197*, 179.
16. Wang, C.; Li, S.-P.; Li, T.-D. *Desalination* **2009**, *249*, 1.
17. Kralj, D.; Brecevic, L.; Kontree, J. *J. Cryst. Growth* **1997**, *177*, 248.
18. Prisciandaro, M.; Olivieri, E.; Lancia, A.; Musmarra, D. *Ind. Eng. Chem. Res.* **2009**, *48*, 10877.
19. Kavitskaya, A.; Skilskaya, M.; Kucheruk, D.; Goncharuk, V. *Ind. Eng. Chem. Res.* **2007**, *46*, 2243.
20. Liu, G. Q.; Huang, J. Y.; Zhou, Y. M.; Yao, Q. Z.; Ling, L.; Zhang, P. X.; Wu, W. D.; Sun, W. *Tenside Surfactants Deterg.* **2012**, *49*, 216.
21. Amjad, Z. *Tenside Surfactants Deterg.* **2005**, *42*, 71.
22. Wurm, F.; Frey, H. *Prog. Polym. Sci.* **2011**, *36*, 1.
23. Cölfen, H. *Macromol. Rapid. Commun.* **2001**, *22*, 219.
24. Antonietti, M.; Breulmann, B.; Goltner, C. G. *Chem.—Eur. J.* **1998**, *4*, 2493.
25. Esselborn, E.; Fock, L.; Knebelkamp, A. *Chem. Macromol. Symp.* **1996**, *102*, 91.
26. Bronstein, L. M.; Sidorov, S. N.; Valetsky, P. M.; Hartmann, J.; Cölfen, H.; Antonietti, M. *Langmuir* **1999**, *15*, 6256.
27. Qi, L.; Cölfen, H.; Antonietti, M. *Angew. Chem. Int. Ed. Engl.* **2000**, *39*, 604.
28. Qi, L.; Cölfen, H.; Antonietti, M. *Chem. Mater.* **2000**, *12*, 2392.
29. Seldak, M.; Antonietti, M.; Cölfen, H. *Macromol. Chem. Phys.* **1998**, *199*, 247.
30. Ling, L.; Liu, G. Q.; Huang, J. Y.; Wang, H. C.; Zhou, Y. M.; Yao, Q. Z.; Cao, K.; Liu, Y. H.; Tu, Y.; Zhou, X. K.; Sun, W.; Wu, W. D. *Tenside Surfactants Deterg.* **2013**, *50*, 14.
31. Jayaraman, A.; Subramanyam, G.; Sinhdu, S.; Ajikumar, P. K.; Valiyaveetti, S. *Cryst. Growth Des.* **2007**, *7*, 142.
32. Cölfen, H.; Antonietti, M. *Langmuir* **1998**, *14*, 582.
33. Xie, A. J.; Zhang, C. Y.; Shen, Y. H.; Qiu, L. G.; Xiao, P. P.; Hu, Z. Y. *Cryst. Res. Technol.* **2006**, *41*, 967.
34. Cölfen, H. *Macromol. Rapid Commun.* **2001**, *22*, 219.
35. Liu, D.; Hui, F.; Lédion, J.; Li, F. *Environ. Technol.* **2011**, *32*, 1017.
36. Chakraborty, D.; Agarwal, V. L.; Bhatia, S. K.; Bellare, J. *Ind. Eng. Chem. Res.* **1994**, *33*, 2187.
37. Liu, G. Q.; Huang, J. Y.; Zhou, Y. M.; Yao, Q. Z.; Ling, L.; Zhang, P. X.; Fu, C. E.; Wu, W. D.; Sun, W. *Tenside Surfactants Deterg.* **2012**, *49*, 216.
38. Gal, J.-Y.; Bollinger, J.-C.; Tolosa, H.; Gache, N. *Talanta* **1996**, *43*, 1497.